Reviews

Thermodynamically stable nanodroplets and nanobubbles

A. K. Shchekin*

Physical Department, St. Petersburg State University,
7/9 Universitetskaya nab., 199034 St. Petersburg, Russian Federation.
E-mail: a.shchekin@spbu.ru

Theoretical results of studying thermodynamic and structural characteristics of free droplets and bubbles around nanosized solid heterogeneous spherical inclusions using phenomenological thermodynamic approach and various versions of the molecular density functional method are reviewed. In the case of a droplet in an undersaturated or supersaturated vapor, the central solid particle is assumed to be lyophilic and can be either electrically charged, or uncharged. In the case of a vapor bubble in a stretched liquid, the central particle is assumed to be lyophobic and, as in the previous case, can be electrically charged or uncharged. The structure of droplets and bubbles is described by equilibrium molecular density profiles. Thermodynamic characteristics imply the chemical potential of molecules in a droplet or bubble as a function of their size, the work of formation of equilibrium droplets or bubbles as a function of the chemical potential of molecules

* Aleksandr Kimovich Shchekin, born in 1957, Doctor of Sciences in Physics and Mathematics, Professor, a honored worker of the higher professional education of the Russian Federation, Corresponding Member of the Russian Academy of Sciences (RAS), Head of the Chair of Statistical Physics of the St. Petersburg State University, and elected a candidate to academicians of the RAS in 2022. A. K. Shchekin is a specialist in the field of the theory of first-order phase transitions, theory of micelle formation, and physical chemistry of surface phenomena. He developed the theory of sign preference in ion-induced nucleation; proposed a method for the calculation of thermodynamic characteristics of small deformed droplets in noncentral electrical fields; constructed the nucleation theory on soluble and insoluble condensation nuclei; calculated thermodynamic characteristics of small droplets around wettable nanoparticles; developed new models of direct and reverse micelles and kinetic description of superfast, fast, and slow relaxation in micellar solutions; described the dynamics of the growth of multicomponent droplets taking into account effects of nonstationarity and excluded volume; constructed the theory of degassing of solutions supersaturated with the gas; and proved the existence of stable vapor bubbles around lyophobic nanoparticles. A. K. Shchekin is the author of 438 scientific works and three monographs, and he was the supervisor of nine candidate dissertations. He is a member of editorial boards of the journals *Doklady RAN. Khimiya, nauki o materialakh* [*Reports of Russian Academy of Sciences. Chemistry, Materials Science*] and *Physica A: Statistical Mechanics and its Applications* and a member of the Executive Committee of the Asian Society for Colloid and Surface Science (ASCASS). A. K. Shchekin was the Vice-Editor-in-Chief of the *Kolloidnyi Zhurnal* (*Colloidal Journal*) up to January 2022.

Published in Russian in *Izvestiya Akademii Nauk. Seriya Khimicheskaya,* Vol. 72, No. 2, pp. 295—311, February, 2023.
1066-5285/23/7202-0295

in the system, and the surface tension and disjoining pressure in droplets or bubbles as functions of its radius.

Key words: droplet, bubble, condensation nucleus, nucleation, density profile, disjoining pressure, surface tension, chemical potential, work of formation.

Introduction

Heterogeneous formation of particles of a new phase on insoluble nanosized solid inclusions is a widely abundant fundamental phenomenon that can be both desirable and undesirable in practice. Conditions for the heterogeneous formation of thermodynamically stable particles of a new phase are discussed in this article. For this purpose, author´s review of the results of theoretical studies performed both in terms of the phenomenological thermodynamic approach and using different versions of the molecular density functional method of the thermodynamic and structural characteristics of free droplets and bubbles around solid nanoparticles is presented below. These studies have been carried out with the participation of the author of this review for more than 25 years since the mid-1990s to 2022. In the case of a droplet condensed in undersaturated or supersaturated vapor, a solid spherical nanoparticle plays the role of the condensation nucleus, which is assumed to be well wettable by the liquid of the droplet (*i.e.*, lyophilic). This nucleus can bear an electrical charge. In the case of formation of a vapor bubble in a stretched liquid (under reduced pressure relative to the liquid—vapor equilibrium), the central particle is assumed to be non-wettable by the surrounding liquid (*i.e.*, lyophobic) and, as in the previous case, can bear an electrical charge. Speaking below about thermodynamic characteristics, we imply the chemical potential of molecules in a droplet or bubble as a function of the external radius of the liquid or vapor shell around the nucleus, the work of formation of an equilibrium droplet or bubble as a function of supersaturation of the system, and the surface tension and disjoining pressure of droplets or bubbles as a function of their radius. The structure of droplets or bubbles in terms of the molecular density functional method is described by equilibrium profiles of the molecular density.

Phenomenological approach to droplets and bubbles

The existence in vapor of thermodynamically stable free spherical small droplets in the form of liquid films around lyophilic solid condensation nuclei was first substantiated in the framework of the thermodynamic theory.[1–3] The main concepts will be clarified briefly. Let a wettable, insoluble, incompressible, and uncharged spherical nucleus of radius R_n is situated at the center of the nucleated droplet of the liquid of radius R (Fig. 1). The nucleated droplet is surrounded from the outside by a vapor—gas medium. It is assumed that the droplet and medium are at the mechanical and thermal equilibrium, but the chemical equilibrium can be absent; *i.e.*, the chemical potential of molecules of the droplet can differ from the chemical potential of vapor molecules.

The disjoining pressure (Π) exists in thin liquid films in which a significant internal overlapping of the surface layers is observed from different sides of the film. For a planar film, Π is equal to[4]

$$\Pi = P_N - P_l(\mu), \qquad (1)$$

where P_N is the normal component of the pressure tensor in the film, which for the planar film coincides with pressure P_g in the gas phase, and $P_l(\mu)$ is the pressure in the bulk liquid at the same values of chemical potential μ and temperature T as those in the film. The disjoining pressure of the planar film depends on the film thickness h and for a stable film is positive.[4]

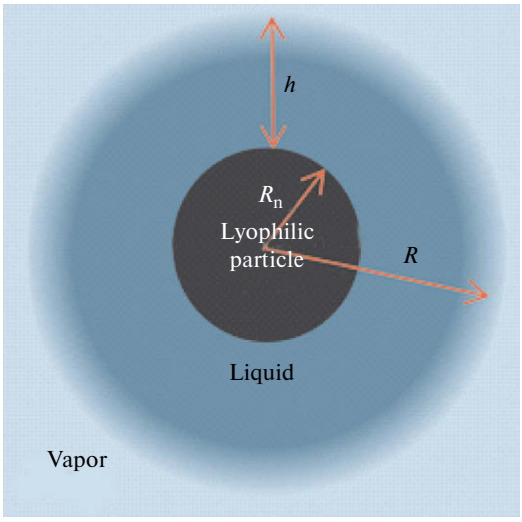

Fig. 1. Droplet of radius R on the wettable solid nucleus of radius R_n; $h = R - R_n$ is the liquid film thicknes.

The chemical potential of condensate molecules in a droplet of radius R will be designated as μ_R. Let us consider the dependence of μ_R on radius R in the situation shown in Fig. 1. For sufficiently small thicknesses $h = R - R_n$, this dependence includes a positive contribution from the capillary pressure of the curved surface of a droplet and a negative contribution from the positive disjoining pressure Π. In the main order for curvature $1/R$, the following can be written[1–3]:

$$\mu_R = \mu_\infty + \frac{1}{\rho_l}\left(\frac{2\gamma}{R} - \Pi(h)\right), \quad (2)$$

where μ_∞ is the chemical potential of the condensate corresponding to the liquid—vapor equilibrium at the planar interface, γ is the mechanically determined surface tension at the liquid—vapor interface, and ρ_l is the density of the number of molecules in the liquid. The $\Pi(h)$ dependence can be taken the same as that for the planar film.

The characteristic behavior of μ_R is illustrated in Fig. 2, where μ is the specified chemical potential of vapor molecules, R_e is the radius of the stable droplet at equilibrium with vapor, R_c is the radius of the unstable (critical) droplet at equilibrium with vapor, and R_{th} is the radius of the droplet at which the maximum value μ_{th} of the chemical potential of the droplet is achieved (radii of the stable and unstable droplets at $\mu = \mu_{th}$ coincide with R_{th}). At $\mu \geq \mu_{th}$, the droplets cannot be at equilibrium with vapor, which means their barrierless nucleation on nuclei and further irreversible growth.

It follows from Fig. 2 that this is the presence of the positive disjoining pressure (giving the ascending branch of chemical potential μ_R) in the droplet which provides (at a specified chemical potential of vapor) two simultaneously existing equilibrium droplet radii in supersaturated vapor (*i.e.*, at $\mu > \mu_\infty$), one radius in saturated and undersaturated vapor (at $\mu \leqslant \mu_\infty$) and also causes the existence of the threshold value μ_{th} of the chemical potential of molecules in vapor and, correspondingly, the threshold degree of supersaturation of vapor beginning from which nucleation on the wettable particles occurs without barrier. If in Eq. (2) the exponential (Π^{exp}) or power (Π^{pow}) approximations of the disjoining pressure isotherms for planar liquid films are used[4]

$$\Pi^{exp}(h) = K\exp(-h/\lambda),\ \Pi^{pow}(h) = A/h^3, \quad (3)$$

where λ is the parameter having a sense of correlation length in the liquid film formed around the nucleus, $K \cong s/\lambda$ is the positive parameter of structural repulsion,[5] s is the coefficient of liquid spreading over the planar surface of the condensation nucleus, and A is the positive parameter directly proportional to the Hamaker constant), then it can be shown[6,7] that this threshold supersaturation decreases with an increase in the nuclei size. This explains condensation in Earth's atmosphere at superlow vapor supersaturations.

The combined conditions concerning the thermodynamic wetting parameters, disjoining pressure isotherms, and condensation nucleus sizes that are required for the formation of liquid films uniformly covering the condensation nucleus were considered in Refs 5, 8, and 9. In addition, the paper[10] published later should be mentioned, where the chemical potential maximum in a droplet was also discussed using the power isotherm of disjoining pressure.

The further extension of the thermodynamic approach[1–3,6,7] to the case of solid wettable condensation nuclei with electrical charges was performed in the work,[11] where the situation of a uniform charge distribution over the nucleus surface is considered. In particular, the equation for the dependence of the chemical potential μ_R of a molecule in the spherical liquid film consisting of polar molecules located on a uniformly charged nucleus on the film thickness, the condensation nucleus radius, and the value and sign of the nucleus charge was derived in the form[11]:

$$\mu_R = \mu_\infty + \frac{1}{\rho_l}\left[\frac{2\gamma}{R} - \frac{1}{8\pi R^4}\left(\frac{1}{\varepsilon_g} - \frac{1}{\varepsilon_l}\right)q^2 + \right.$$
$$\left. + \frac{k_1}{R^5}q^2 + \frac{4k_2}{3R^7}q^3 - \Pi(h)\frac{R_n^2}{R^2}\right], \quad (4)$$

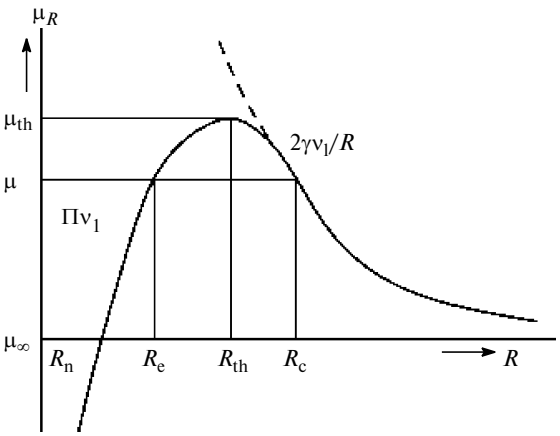

Fig. 2. Chemical potential μ_R *vs* droplet radius (for clarification, see text), $v_l = 1/\rho_l$.

where ε_g and ε_l are the dielectric constants in the gas and liquid phases, q is the total nucleus charge, and k_1 and k_2 are the coefficients at the linear and square contributions of induction to the excess polarization at the liquid—vapor interface. Equation (4) can be considered as a generalization of the classical equation derived by J. J. Thomson[12] into which Eq. (4) transforms if we assume $k_1 = 0$, $k_2 = 0$, and $\Pi = 0$. The qualitative behavior of μ_R as a function of the droplet radius R determined by Eq. (4) is analogous to that shown in Fig. 2, but the presence of the central charge increases the size of a stable droplet and decreases the threshold value of chemical potential μ_{th}. If assuming $q = 0$, then the presence of factor R_n^2/R^2 in front of disjoining pressure $\Pi(h)$ in the right part of Eq. (4) refines the corresponding contribution in Eq. (2).

The theory was also extended over an interesting case where the charge is adsorbed in the form of the ion on the nucleus surface.[13,14] In this case, the spherical symmetry of a droplet is violated, and the problem on the determination of the non-spherical profile $r(\theta)$ of a droplet and chemical potential of a molecule in the liquid film becomes substantially more complicated (Fig. 3). The differential equation of the mechanical equilibrium of a curved film[15,16] was taken as the equation for the droplet profile. In the case considered, this equation can be written as the following differential equation:

$$\frac{2\gamma}{\left(r^2(\theta)+r_\theta^2\right)^{1/2}}\left(2+\frac{r^2(\theta)+r(\theta)r_{\theta\theta}}{r^2(\theta)+r_\theta^2}-\frac{r_\theta}{r(\theta)}\mathrm{ctg}\theta\right)-$$
$$-\Pi(r(\theta)-R_n)\frac{R_n^2}{r(\theta)\left(r^2(\theta)+r_\theta^2\right)^{1/2}}=P_l(\mu)-P_g(\mu)+$$
$$+\frac{\varepsilon_l(\nabla\varphi_l)^2\Big|_{r=r(\theta)}-\varepsilon_g(\nabla\varphi_g)^2\Big|_{r=r(\theta)}}{8\pi}+$$
$$+\frac{\varepsilon_g(\nabla\varphi_g,\vec{n})^2\Big|_{r=r(\theta)}-\varepsilon_l(\nabla\varphi_l,\vec{n})^2\Big|_{r=r(\theta)}}{4\pi}, \qquad (5)$$

where $r_\theta \equiv dr(\theta)/d\theta$, $r_{\theta\theta} \equiv d^2r(\theta)/d\theta^2$, $P_l(\mu)$, and $P_g(\mu)$ are the pressures in the bulk liquid and in the gas in the absence of a charge but at the same chemical potential μ and temperature T as in the film in the presence of a charge, φ_l and φ_g are the electrical potentials in the liquid and gas phases in the presence of an adsorbed ion in the geometry shown in Fig. 3, and $\vec{n}$ is the unit normal to the droplet surface. The combined numerical solution of Eq. (5) and Laplace equation for the electrical potential in the case of low deviations $|r(\theta) - R|/R << 1$, where R is the equivalent radius of the sphere the volume of which is equal to the droplet volume, made it possible[13,14] to determine the droplet shape in the noncentral electrical field and to find the expression for the chemical potential of condensate molecules in the film as a function of the equivalent curvature radius of the film external surface. The exponential (Π^{exp}) and power (Π^{pow}) approximations (3) of the disjoining pressure isotherms for planar liquid films and the two-exponential approximation[4] $\Pi^{2exp}(h) = K_1\exp(-h/\lambda_1) + K_2\exp(-h/\lambda_2)$ with the coefficients K_1 and K_2 having opposite signs, which corresponds to the partial wetting of the planar solid surface in the absence of an electrical charge, are used in these calculations.

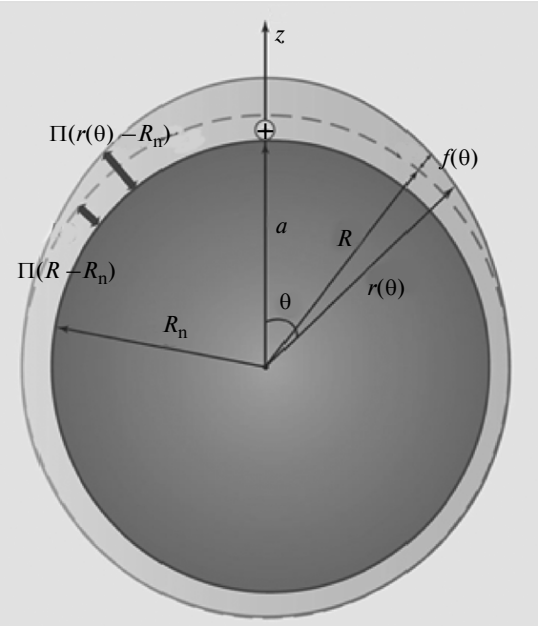

Fig. 3. Droplet on the condensation nucleus with the localized adsorbed ion; a is the distance from the ion to the center of the condensation nucleus, R is the equivalent radius of the sphere, the volume of which is equal to the droplet volume, and $f(\theta) \equiv r(\theta) - R$. Adsorbed ion is designated by a circle with sign + inside.

Figure 4 illustrates the results obtained for the chemical potential of a molecule in a droplet in the case of power approximation Π^{pow} determined by Eq. (3). The following values of parameters were taken[14] for the calculation in Fig. 4: $T = 300$ K, $v_l = 3.3 \cdot 10^{-29}$ m^3, $\gamma = 0.07$ N m^{-1}, $\varepsilon_g = 1$, $\varepsilon_l = 80$, dielectric constant of the nucleus $\varepsilon_n = 40$, adsorbed ion charge $q = e = 4.8 \cdot 10^{-10}$ electrostatic units of charge, and $A = 5 \cdot 10^{-16}$ erg. According to the cal-

culation results for the power approximation Π^{pow} of the disjoining pressure, the presence of an elementary charge on the surface or at the center of the nucleus stops to affect the maximum of the chemical potential of condensate molecule already for nuclei of radius 3.0—3.5 nm. The distinction of effects of the central and adsorbed elementary charge disappears even earlier: for radii of 2.0—2.5 nm. For smaller particles, the adsorbed charge effects already differ from the central charge effects: they appear as a decrease in the threshold values of chemical potential and vapor supersaturation corresponding to the maxima of the curves in Fig. 4 for barrierless nucleation and as an increase in the size of equilibrium droplets corresponding to the ascending branch of the chemical potential at the left from the maximum μ_R.

Let us now consider heterogeneous vapor bubbles in the stretched liquid including the central solid lyophobic particle (Fig. 5). Evidently, the system we are interested in (nucleus—vapor interlayer—liquid) is contrary, in certain sense, to that shown in Fig. 1. It is well known[17] that bubbles contacting with hydrophobic and hydrophilic solid particles plays an important role in the flotation separation of finely dispersed suspensions (in particular, for mineral raw materials mining) and that the size of particles and properties of their surface exert a substantial effect

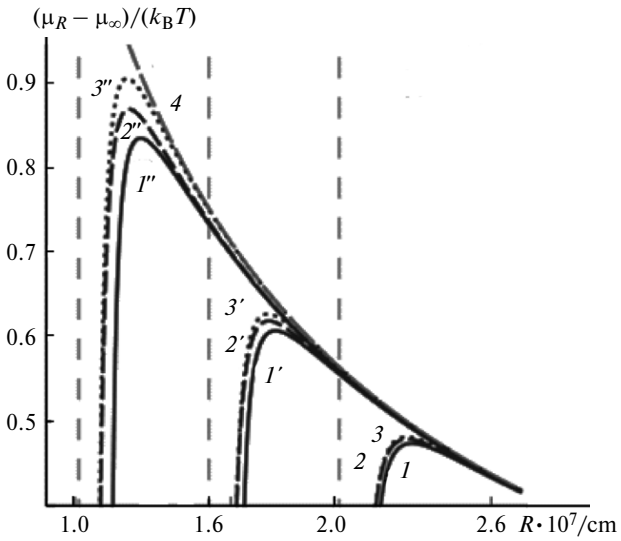

Fig. 4. Shifted dimensionless chemical potential of the molecule in the droplet *vs* film radius R for the isotherm of disjoining pressure Π^{pow} at different radii of the condensation nucleus R_n marked by vertical lines: (*1*, *1′*, *1″*) at fixed distance $a - R_n = 1 \cdot 10^{-10}$ cm of the adsorbed ion from the particle surface; (*2*, *2′*, *2″*) for the charge of the same value located at the center of the nucleus; (*3*, *3′*, *3″*) for the uncharged nucleus; and (*4*) taking into account only the contribution associated with the excess Laplace pressure.

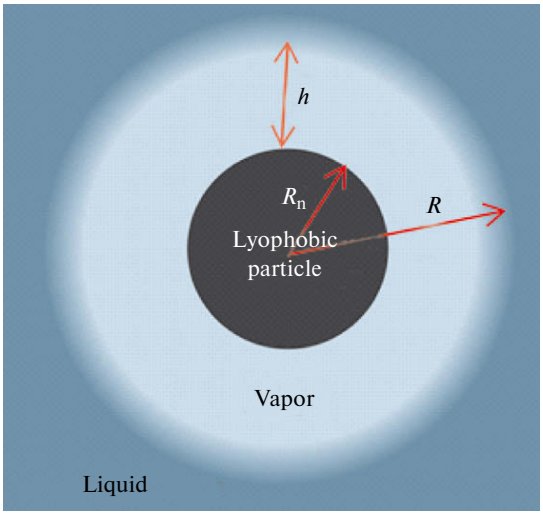

Fig. 5. Bubble of radius R on the lyophobic nucleus of radius R_n; $h = R - R_n$ is the vapor interlayer thickness.

on the flotation characteristics of mineral particles. A number of works[18,19] is devoted to the discussion of these characteristics, where rather large bubbles with small lyophilic or lyophobic solid particles adsorbed on the surface were considered. We are interested in ultrasmall heterogeneous vapor bubbles around lyophobic particles, since it was mentioned[6] that strong lyophobicity of the nucleus surface should be a condition for the existence of a stable free bubble around a solid particle in the stretched or overheated liquid. However, more detailed thermodynamic consideration of free bubbles around lyophobic particles has not been performed until recently. Homogeneous stable bubbles in confined systems [20—28] and stable sessile bubbles in the presence of pinning [29—33] are discussed, but a commonly accepted explanation of the stability of nanobubbles in bulk phases is still lacking.

Direct calculations of structural and thermodynamic characteristics of droplets and bubbles

Evidently, possibilities of the phenomenological approach to the description of droplets and bubbles are restricted by the fact that in nanosized particles of the new phase the bulk properties of the phase can be unachievable. In particular, the use of tabulated values of the surface tension and the disjoining pressure isotherms for planar films (in the case of the films on wettable spherical solid particles) is limited when the particle radius decreases.[15,16] These limits

along with the escape beyond them can be established only in the framework of molecular models of statistical thermodynamics. The molecular density functional is one of the modern methods for the direct calculation of structural and thermodynamic characteristics of nanodroplets and nanobubbles.[34,35]

An explicit expression for the grand thermodynamic potential $\Omega[\rho(\vec{r})]$ of a droplet—vapor or bubble—liquid system as a functional of the local density $\rho(\vec{r})$ of the number of fluid molecules at the point with radius $\vec{r}$ is specified in terms of the molecular density functional method. The fluid in the bulk part of the system can be in the state of vapor or liquid. The equilibrium profiles $\rho_e(\vec{r})$ of the fluid density obtained as a result of the solution of the variation problem $\delta\Omega[\rho(\vec{r})]/\delta\rho(\vec{r})|_{\rho=\rho_e} = 0$ and corresponding to the saddle point of the grand thermodynamic potential characterize the unstable equilibrium of particles of the new phase. These particles act as critical nuclei of the new phase at a specified value of the chemical potential of fluid molecules and have a short lifetime. If there are equilibrium density profiles $\rho_e(\vec{r})$ corresponding to the minimum of the grand thermodynamic potential of the system, they characterize the stable equilibrium of particles of the new phase. As we have seen in the thermodynamic analysis of heterogeneous droplets on wettable condensation nuclei in the previous section, these particles can exist for an unrestrictedly long time even in the undersaturated vapor.

The first results obtained by the molecular density functional method for heterogeneous droplets were presented in Refs 36—41. The numerical calculations of the radial profiles were performed in Refs 42 and 43 for the lyophilic particle—liquid film—vapor system at different values of the chemical potential of vapor. The gradient method[39] of the molecular density functional was used, in terms of which the grand thermodynamic potential of the system in the presence of the liquid film on the charged condensation nucleus was specified as follows[42,43]:

$$\Omega = \int\left[f_{hs}(\rho) - a\rho^2 - \mu\rho + \frac{C}{2}(\nabla\rho)^2 + \right.$$
$$\left. + \frac{(Ze)^2}{8\pi\varepsilon(\rho,T)r^4} + \rho w_{nf}(r)\right] d\vec{r}. \qquad (6)$$

Integration in Eq. (6) does not involve the nucleus volume. Here $f_{hs}(\rho)$ is the free energy density of molecules interacting as solid spheres, $\rho(\vec{r})$ is the local density of the fluid at the point specified by radius $\vec{r}$ in the coordinate system the center of which coincides with the solid nucleus center, a is the parameter of attraction of fluid molecules in the mean field approximation related to the long-range component of the intermolecular potential and, in particular, to the energy parameter $\varepsilon_{ff} = a/\sigma^3$ for fluid molecules, μ is the chemical potential of fluid molecules, C is the parameter that depends on the absolute temperature T and is related to the surface tension γ_∞ at the planar interface of the liquid and gas phases (can approximately be calculated as $C = 14\sigma^5 k_B T$), k_B is the Boltzmann constant, Z is the charge of the condensation nucleus in elementary charge units e, $\varepsilon(\rho(\vec{r}), T)$ is the local value of static dielectric permeability specified as the known function of the temperature and local density of the fluid, and $w_{nf}(r)$ is the total potential of interaction of the nucleus with the fluid molecule (integral sum of interactions with all molecules of the nucleus). Note that the electrical contribution in Eq. (6) does not describe the effect of sign preference for nucleation on positively and negatively charged particles related to an excess spontaneous surface polarization. As shown previously,[11] this effect is small for nanosized particles.

For the free energy density $f_{hs}(\rho)$ of solid spheres, we chose[42,43] the van der Waals[39]

$$f_{hs}^{VdW}(\rho) = k_B T\rho\left[\ln(\lambda_{th}^3\rho) - 1 - \ln(1 - v_0\rho)\right] \qquad (7)$$

and Carnahan— Starling models[44]

$$f_{hs}^{CS}(\rho) = k_B T\rho\left[\ln(\lambda_{th}^3\rho) - 1 + \frac{4\eta - 3\eta^2}{(1-\eta)^2}\right], \qquad (8)$$

where v_0 is the excluded-volume parameter, $\lambda_{th} = \lambda_{th} = \hbar\sqrt{2\pi/(mk_B T)}$ is the thermal length of de Broglie wave ($\hbar$ is Planck′s constant, m is the mass of the fluid molecule), and $\eta = \pi d^3\rho/6$ is the dimensionless molecular density of the fluid (d is the diameter of the molecule in the model of solid spheres). The potential of the interaction of the nucleus with the fluid molecule $w_{nf}(r)$ was taken in the following form[45]:

$$w_{nf}(r) = \frac{4\pi\varepsilon_{nf}\rho_n\sigma^3}{5}\left\{\frac{\sigma}{8r}\left[\frac{\sigma^8}{(r+R_n)^8} - \frac{\sigma^8}{(r-R_n)^8} + \right.\right.$$
$$+ 10\sigma^2\left(\frac{1}{(r-R_n)^2} - \frac{1}{(r+R_n)^2}\right)\Bigg] +$$
$$+ \frac{5}{6}\sigma^3\left(\frac{1}{(r+R_n)^3} - \frac{1}{(r-R_n)^3}\right) +$$
$$\left. + \frac{\sigma^9}{9}\left(\frac{1}{(r-R_n)^9} - \frac{1}{(r+R_n)^9}\right)\right\}, \qquad (9)$$

where ε_{nf} is the Lennard-Jones energy parameter for the interaction of solid body and fluid molecules, ρ_n is the average molecular density of the solid body, $\sigma = (\pi/6)^{1/3}d$, and R_n is the nucleus radius. The following values were taken for the lyophilic nucleus[43]: $\rho_n = 2.66 \cdot 10^{28}$ m^{-3} (density of quartz) and the ratio of the energy parameters $\varepsilon_{nf}/\varepsilon_{ff} = \varepsilon_{nf}\sigma^3/a = 2$.

The numerical calculation results for the density profiles in equilibrium argon droplets in the presence of capillary, electrostatic, and molecular forces[43] is shown in Fig. 6. At a specified chemical potential, curves *1* and *5* correspond to two profiles around the uncharged condensation nucleus ($Z = 0$) in the presence of potential $w_{nf}(r)$, curves *2* and *4* correspond to two profiles around the charged nucleus at $Z = 2$ and $w_{nf}(r) = 0$, curves *3* and *6* correspond to two profiles around the charged nucleus at $Z = 2$ in the presence of potential $w_{nf}(r)$; and curve *7* corresponds to droplets without nucleus at $Z = 0$, $w_{nf}(r) = 0$, and $R_n = 0$. The profile in the form of a classical step for droplets formed at homogeneous nucleation, when an equimolecular surface is chosen as a separating surface, is also shown in Fig. 6.

The minima of the grand thermodynamic potential Ω (see Eq. (6)) correspond to profiles *1* and *3* in Fig. 6, and these profiles characterize stable droplets on the condensation nuclei. Profiles *5*—*7* refer to the maxima Ω and describe critical droplets unstable toward a change in the number of molecules in them.

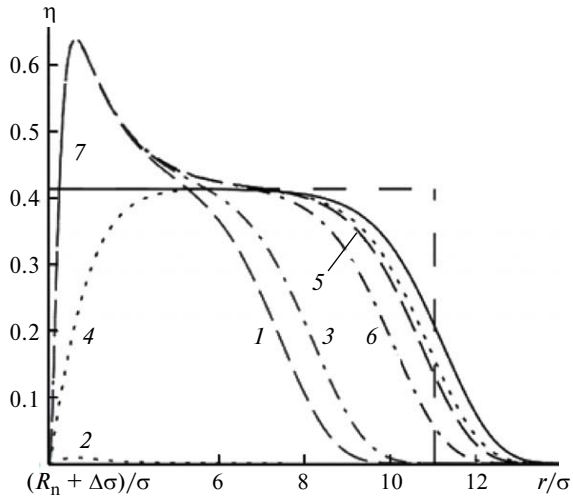

Fig. 6. Equilibrium dimensionless density profiles $\eta(r)$ of the number of molecules in argon droplets in supersaturated vapor at $T = 90$ K and at dimensionless shift $(\mu - \mu_\infty)/k_BT = 0.27$ of the chemical potential of argon molecules from its binodal value[43] (for clarifications, see text). Accepted in calculations: $\sigma = 2.53 \cdot 10^{-10}$ m, $\Delta\sigma = 0.62\sigma$, $R_n = 2\sigma$, and $a = 3.58 \cdot 10^{-49}$ J m^3.

It is seen from Fig. 6 that the profiles of stable and critical droplets at a specified slight deviation of the chemical potential from its value on the binodal nearly coincide for $r/\sigma < 5$, and the profile maxima appreciably exceed the density of the bulk liquid. This means that the influence of the molecular interaction with the nucleus becomes predominant near the condensation nucleus.

At the same time, when only the Coulomb electrical field of the nucleus is taken into account at $w_{nf}(r) = 0$, density profile *2* formally corresponding to the stable droplet and profile *4* for the critical droplet near the condensation nucleus do not exceed the bulk vapor density. This droplet cannot be considered as a uniformly covering particle. Thus, we are in contradiction with an assumption about the radial symmetry of the system and, correspondingly, profiles *2* and *4* have no physical sense.

The fact that the maximum of profile *1* in Fig. 6 noticeably exceeds the bulk density of the liquid phase at the ratio of energy parameters $\varepsilon_{nf}\sigma^3/a = 2$ means the full wetting of the nucleus surface in the presence of these molecular forces. The influence of the $\varepsilon_{nf}\sigma^3/a$ ratio on the behavior of the profiles of equilibrium droplets was studied.[46] The results are shown in Fig. 7. It is seen that an increase in the energy parameter ε_{nf} for the particle—condensate molecular interaction leads to an increase in the

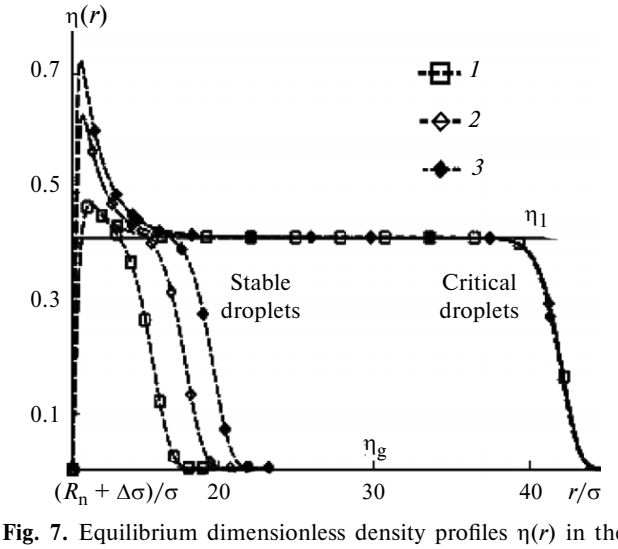

Fig. 7. Equilibrium dimensionless density profiles $\eta(r)$ in the argon droplet in supersaturated vapor in the absence of an electrical charge of the nucleus; $\varepsilon_{nf} = 2a/\sigma^3$ (*1*), $6a/\sigma^3$ (*2*), and $12a/\sigma^3$ (*3*). Temperature $T = 90$ K and $(\mu - \mu_\infty)/(k_BT) = 0.073$. Accepted in calculations: $\sigma = 2.53 \cdot 10^{-10}$ m, $\Delta\sigma = 0.62\sigma$, $R_n = 10\sigma$, and $a = 3.58 \cdot 10^{-49}$ J m^3. Horizontal lines correspond to the bulk density values for the gas and liquid phases.

density peak in the first molecular layer around the nucleus.

When the chemical potential increases, the profiles of stable and critical droplets approach each other and merge at some threshold value μ_{th} as it was predicted by the thermodynamic theory.[5,11] No solution of the variation problem $\delta\Omega[\rho(\vec{r})]/\delta\rho(\vec{r})|_{\rho=\rho_e} = 0$ exists in the form of the equilibrium droplet profile above the μ_{th} value, and the lyophilic nucleus—supersaturated vapor system is unstable toward the spontaneous condensation on the nucleus.

If radius R_{em} of the equimolecular separating droplet—vapor surface is determined by the equation

$$R_{em}^3 = \frac{\rho_l}{\rho_l - \rho_g} R_n^3 - \frac{1}{\rho_l - \rho_g} \int_{R_n}^{\infty} dr r^3 \frac{d\rho(r)}{dr}, \qquad (10)$$

then the dependence of the chemical potential of a molecule in the droplet on the equimolecular radius of the equilibrium heterogeneous droplet taking into account the action of capillary, electrostatic, and molecular forces can be determined from the equilibrium profiles $\rho(r)$ at different μ values using Eq. (10). This dependence is shown in Fig. 8.[46]

Figure 8 shows that all curves of the chemical potential of the molecule in the equilibrium heterogeneous droplet lie below the curve of the chemical potential of the molecule in the homogeneous droplet (the case of $R_n = 0$, $Z = 20$, $\varepsilon_{nf} = 0$). At high nucleus charges without molecular field of the nucleus ($Z = 0$, $\varepsilon_{nf} = 0$), the chemical potential curve approaches the curve specified by J. J. Thomson´s curve.[12] However, the $(\mu_{R_{em}} - \mu_\infty)/(k_B T)$ dependences with allowance for the molecular field deviate still more and more strongly from this curve as wetting increases with an increase in ε_{nf} of the nucleus. Figure 8 also shows that the presence of an electrical charge and an increase in the lyophilicity of the nucleus decrease the chemical potential maximum for fluid molecules in the droplet and, correspondingly, decrease the threshold value μ_{th} of the chemical potential of vapor for barrierless heterogeneous nucleation.

In terms of the phenomenological thermodynamic theory, the existence of stable equilibrium heterogeneous droplets is caused by the disjoining pressure in thin liquid films. The fact that the determined by the density functional method dependences of chemical potential $\mu_{R_{em}}$ on radius R_{em} of the droplet qualitatively coincide with the predictions of the thermodynamic theory considered in the previous section made it possible to calculate[46,47] the disjoining pressure isotherms in strongly curved liquid films. The disjoining pressure isotherms were obtained[46] using Eq. (4) at $k_1 = 0$, $k_2 = 0$, and calculated dependence $(\mu_{R_{em}} - \mu_\infty)/(k_B T)$ for $\varepsilon_{nf}\sigma^3/a = 6$ and at different nucleus radii R_n (Fig. 9).

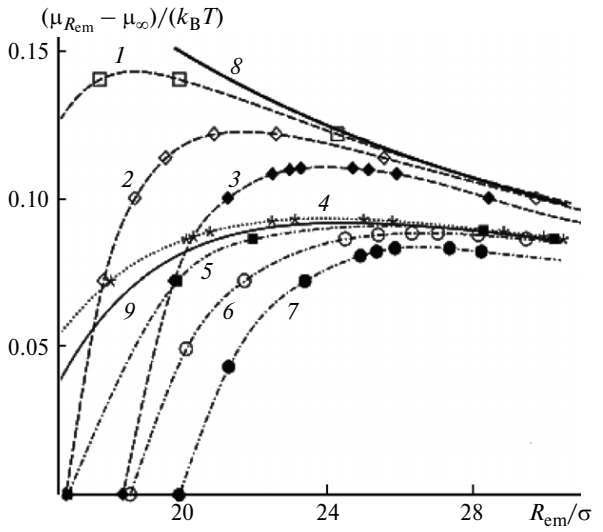

Fig. 8. Dependences of the shifted dimensionless chemical potential $(\mu_{R_{em}} - \mu_\infty)/(k_B T)$ of the molecule in the argon droplet *vs* equimolecular radius R_{em}/σ at different ratios $\varepsilon_{nf}\sigma^3/a$ and nucleus charges: $\varepsilon_{nf} = 2a/\sigma^3$, $Z = 0$ (*1*); $\varepsilon_{nf} = 6a/\sigma^3$, $Z = 0$ (*2*); $\varepsilon_{nf} = 12a/\sigma^3$, $Z = 0$ (*3*); $\varepsilon_{nf} = 0$, $Z = 20$ (*4*); $\varepsilon_{nf} = 2a/\sigma^3$, $Z = 20$ (*5*); $\varepsilon_{nf} = 6a/\sigma^3$, $Z = 20$ (*6*); $\varepsilon_{nf} = 12a/\sigma^3$, $Z = 20$ (*7*); $\varepsilon_{nf} = 0$, $Z = 0$, $R_n = 0$ (*8*); and the dependence calculated by J. J. Thomson´s equation (*9*). Accepted in calculations: $T = 90$ K, $R_n = 10\sigma$, $\sigma = 2.53 \cdot 10^{-10}$ m, and $a = 3.58 \cdot 10^{-49}$ J m^3.

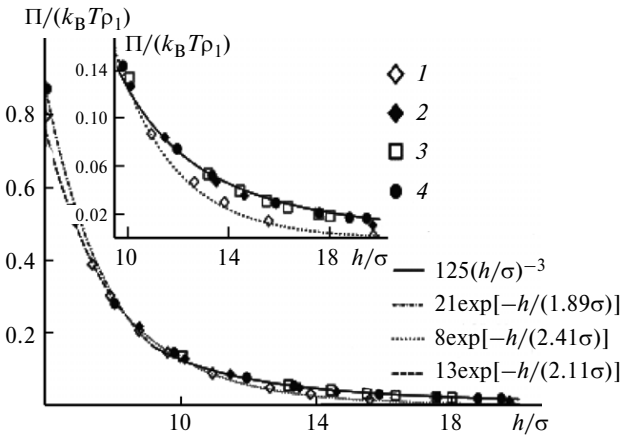

Fig. 9. Dimensionless disjoining pressure $\Pi/(k_B T \rho_l)$ in an argon droplet on the uncharged spherical solid nucleus ($Z = 0$) as a function of the dimensionless thickness of the liquid film $h/\sigma = (R_{em} - R_n)/\sigma$ at different nucleus radii: $R_n = 10\sigma$ (*1*), 20σ (*2*), 30σ (*3*), and 50σ (*4*). Accepted in calculations: $T = 90$ K, $\sigma = 2.53 \cdot 10^{-10}$ m, and $a = 3.58 \cdot 10^{-49}$ J m^3; nucleus wetting was specified by the equation $\varepsilon_{nf}\sigma^3/a = 6$. Inset: amplified fragment of the plot.

It is seen from Fig. 9 that the disjoining pressure decreases nearly to zero at $h/\sigma > 18$. Such a fast decrease in the disjoining pressure for droplets on small uncharged and charged solid nuclei was considered[6,11,48–50] earlier as satisfying the thermodynamic theory. A similar behavior of the $\Pi(h)$ isotherms was also obtained[37,40] for droplets on uncharged nuclei in terms of the nonlocal method of the molecular density functional.

As follows from Fig. 9, the disjoining pressure curves for larger nuclei nearly coincide. This can be explained by the fact that for these solid nucleus sizes the disjoining pressure approaches the limit of the solid body—condensate planar interface and remains unchanged with the further increase in the size of the condensation nucleus. For greater thicknesses, all points at $R_n > 20\sigma$ can be approximated by the power approximation $\Pi^{pow}(h) = 125k_BT\rho_l(h/\sigma)^{-3}$. The exponential approximation $\Pi^{pow}(h) = 13k_BT\rho_l \times \exp[-h/(2.11\sigma)]$ gives the best correspondence for smaller thicknesses at $5\sigma < h < 9\sigma$. Note that the change of the exponential descend of the disjoining pressure for small thickness of droplets by a power descend for great thicknesses is in accordance with the predictions of the thermodynamic theory.[6,7]

According to Refs 15 and 16, the condition of mechanical equilibrium of the spherical wetting film of the liquid on the spherical solid at choosing the equimolecular surface film as the external separating surface can be written as follows:

$$P_l(\mu) = P_g(\mu) + \frac{2\gamma_{em}}{R_{em}(\mu)} - [P_N(r_i) - P_l(\mu)]\left(\frac{r_i}{R_{em}(\mu)}\right)^2, \quad (11)$$

where $P_N(r_i)$ is the normal component of the pressure tensor inside the curved film in internal point r_i of the liquid part of the film near the solid substrate, and γ_{em} is the surface tension for the equimolecular surface; and all values were determined at a specified chemical potential for molecules in the film. The difference $(P_N(r_i) - P_l(\mu))$[15,16,51] was proposed to identify with the mechanical determination of the disjoining pressure for the spherical film

$$\Pi^{(m)}(R_{em} - R_n) \equiv P_N(r_i) - P_l(\mu). \quad (12)$$

Note that in addition to the mechanical determination we can thermodynamically determine the disjoining pressure from the equation followed from Eq. (11):

$$\Pi^{(t)}(h_{em}) = \left(\frac{2\gamma_{em}}{R_{em}} + P_g(\mu) - P_l(\mu)\right)\frac{R_{em}^2}{r_i^2}. \quad (13)$$

The normal component of the pressure tensor $P_N(r)$ in the spherical liquid film can be calculated independently by the density functional method and, hence, $\Pi^{(m)}(R_{em} - R_n)$ can be found independently as a function of the film thickness $h = R_{em} - R_n$. In Eq. (12), position r_m of the $P_N(r_i)$ maximum achieved near the solid nucleus surface or point r_d, where the density profile intersects the line of the volume density of the liquid (see Fig. 7), seem reasonable to be chosen as radius r_i. The results of calculations[47] by Eq. (12) for argon at several values of chemical potential μ (and corresponding R_{em}, r_m, and r_d values) are shown in Fig. 10. The disjoining pressure of the argon film on the planar solid substrate is also shown for comparison. As can be seen from Fig. 10, the results for the mechanical (when using Eq. (12)) and thermodynamic (when using Eq. (13)) determinations of disjoining pressures are very close. The disjoining pressure in a stable droplet depends on the solid nucleus size and is lower (for each nucleus size)

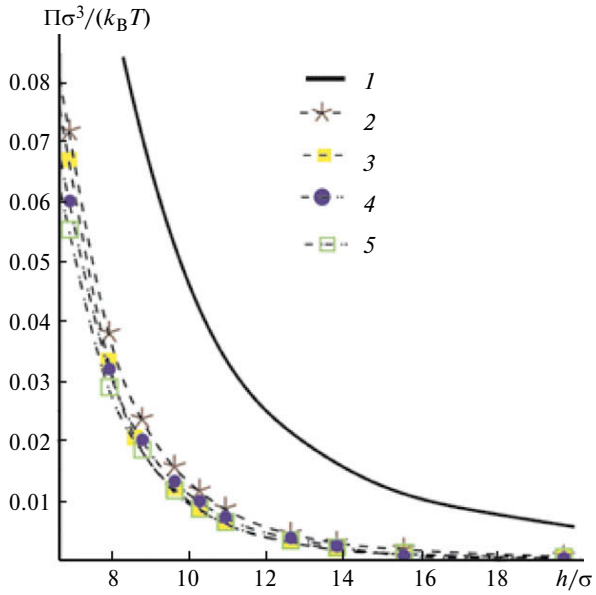

Fig. 10. Dimensionless disjoining pressure $\Pi\sigma^3/(k_BT)$ in an argon droplet on the uncharged spherical solid nucleus as a function of the dimensionless thickness of the liquid film $h/\sigma = (R_{em} - R_n)/\sigma$ depending on the choice of r_i and mechanical (see Eq. (12)) or thermodynamic (see Eq. (13)) determination: planar film (*1*); $\Pi^{(m)}$ and $r_i = r_m$ (*2*); $\Pi^{(m)}$ and $r_i = r_d$ (*3*); $\Pi^{(t)}$ and $r_i = r_m$ (*4*); $\Pi^{(t)}$ and $r_i = r_d$ (*5*). Accepted in calculations: $T = 90$ K, $R_n = 10\sigma$, $\sigma = 2.53 \cdot 10^{-10}$ m, and $a = 3.58 \cdot 10^{-49}$ J m^3; nucleus wetting was specified by the equation $\varepsilon_{nf}\sigma^3/a = 6$.

than the disjoining pressure for the planar liquid film. The lower R_n, the lower the disjoining pressure at the same film thickness. As it was expected, the dependence of Π on the choice of point r_i is weak.

There is knowingly no separation of surface layers nucleus—liquid and liquid—vapor by the bulk liquid interlayer in the case of the equilibrium stable droplet around the wettable nucleus. For droplets on nanosized nuclei, the disjoining pressure makes the main contribution to the overlapping of surface layers, and the dependence of the surface tension of the droplet on the external radius can be neglected against the background of the disjoining pressure. The concept of disjoining pressure loses sense for nuclei of molecular size, and the dependence of the surface tension of the droplet on its radius can be substantial. However, the problem of determining the radius of the solvate shell for the nucleus in the droplet arises in this case as well. The profiles of density and thermodynamically determined surface tension for equilibrium and critical droplets at several sizes of uncharged and charged condensation nuclei which were smaller and larger than molecules of the condensed substance were calculated in the framework of the gradient method of the molecular density functional.[52] The calculations were performed for argon droplets at different chemical potentials of the molecules. The long-range Coulomb potential of electrical forces was additionally taken into account in the case of ion. The obtained dependences of the surface tension of these droplets on their size are comparable with the dependence of the surface tension on the size of the droplet without condensation nucleus. In particular, it was shown[52] that when defining the boundary of the first solvate layer around the condensation nucleus as a point of intersecting of the density profile $\rho(r)$ with the density line ρ_l of the liquid phase at a specified chemical potential of the molecules, the curves of the surface tension dependence on the radius of the equimolecular surface of a small droplet without and with the condensation nucleus correspond to the square (with respect to the droplet curvature) $c = 1/R_{em}$ approximation[53,54]

$$\gamma(c) = \gamma_\infty\left(1 - 2\delta_\infty c + \varkappa c^2\right), \qquad (14)$$

where γ_∞ is the surface tension for the liquid—vapor planar interface. At $T = 90$ K for an argon droplet without nucleus, the Tolman length (δ_∞) is $\delta_\infty = -0.19\sigma$ and the effective rigidity constant ($\varkappa$)[55,56] of the surface layer is $\varkappa = -1.58\sigma^2$. For the particle of radius $R_n = 0.4\sigma$ at the same temperature and lyophilicity of the nucleus specified by the ratio $\varepsilon_{nf}\sigma^3/a = 12$, the following values were obtained[52]: at $Z = 0$, $\delta_\infty = -0.25\sigma$ and $\varkappa = -3.70\sigma^2$; at $Z = 1$, $\delta_\infty = -0.23\sigma$ and $\varkappa = -2.90\sigma^2$; at $Z = 2$, $\delta_\infty = -0.21\sigma$ and $\varkappa = -2.12\sigma^2$. It is seen that the influence of the molecular field and electrical field of the nucleus slightly affects the Tolman length but appreciably changes the effective rigidity constant of the surface layer.

Now let us consider the results of studying spherical shell vapor interlayers (or concentric nanobubbles) around lyophobic surfaces within the molecular density functional method. Such studies and calculations of the structure and thermodynamic characteristics of nanobubbles around lyophobic surface in the stretched liquid were recently performed in Refs 57—60. The equilibrium molecular density profiles around lyophobic nanoparticles (without and with an electrical charge) in the stretched argon-like liquid ($\mu < \mu_\infty$) were calculated. As for the calculation of profiles of heterogeneous droplets,[42—47,52] the grand thermodynamic potential of the system Ω in the presence of a vapor film around the charged nucleus was specified by functional (6) using a combination of the Carnahan—Starling model (8), the mean-field model for the interaction of fluid molecules, and the full Lennard-Jones potential of interaction between the nucleus and fluid molecule (9). Lyophobicity of the particle was controlled by the ratio of energy parameters $\varepsilon_{nf}/\varepsilon_{ff}$ of the attraction of the nucleus molecules and fluid molecules.

The following values were taken[57] for the lyophobic nucleus: $\rho_n = 1.07 \cdot 10^{27}$ m^{-3} (density of paraffin) and ratio of energy parameters $\varepsilon_{nf}/\varepsilon_{ff} \le 0.2$. The calculation results[57] for the molecular profiles in the case of uncharged nucleus ($Z = 0$) at $\varepsilon_{nf}/\varepsilon_{ff} = 0.2$ are given in Fig. 11.

It is seen from Fig. 11 that there are two equilibrium radial density profiles corresponding to two different concentric vapor shells around the solid nucleus at each of three considered values of chemical potential of the fluid below its value for the liquid—vapor equilibrium with the planar interface. At lower values of $|\mu - \mu_\infty|/(k_B T)$, one of these profiles is narrow and another is broad, but the difference in widths becomes lower with an increase in $|\mu - \mu_\infty|/(k_B T)$. The insertion of the found profiles into Eq. (6) for the grand thermodynamic potential

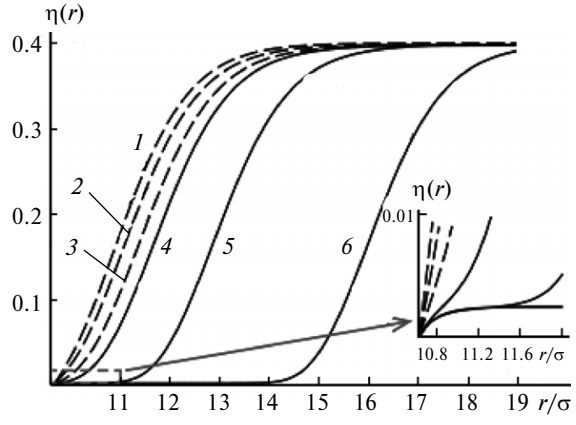

Fig. 11. Equilibrium dimensionless density profiles $\eta(r) = \sigma^3\rho(r)$ in a bubble around a lyophobic particle in the stretched liquid in the absence of an electrical charge of the nucleus at three values of the shift $b = (\mu - \mu_\infty)/(k_BT)$ of the chemical potential of fluid molecules: $b = -0.174$ (*1*, *6*); -0.225 (*2*, *5*); and -0.235 (*3*, *4*); $\varepsilon_{nf}/\varepsilon_{ff} = 0.2$, $R_n = 10\sigma$. Inset: region of low densities near the lyophobic nucleus surface. Temperature 90 K. Accepted in calculations: $\sigma = 2.53 \cdot 10^{-10}$ m, $a = 3.58 \cdot 10^{-49}$ J m^3, $\Delta\sigma = 0.62\sigma$.

Ω showed that the narrower shell is related to the minimum $\Omega = \Omega_{min}$ and represents a stable nanobubble, whereas the broader shell corresponds to the maximum $\Omega = \Omega_{max}$ and refers to the unstable critical nanobubble. From the viewpoint of heterogeneous nucleation,[6,7] the difference $\Omega_{max} - \Omega_{min}$ is the most important characteristic since determines the activation barrier for the spontaneous nucleation of a critical bubble on the lyophobic nucleus. The fact that there is a value of chemical potential at which this difference reaches zero means that beginning from this value the activation barrier for the nucleation of heterogeneous bubbles on lyophobic particles disappears (Fig. 12).

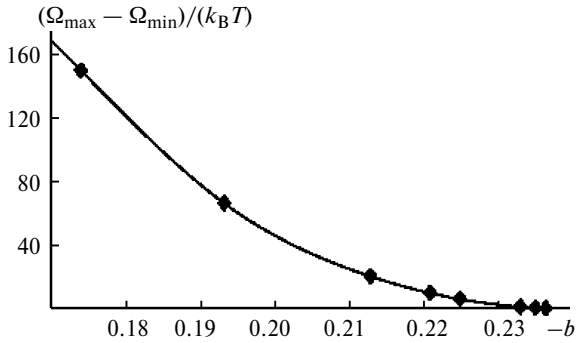

Fig. 12. Dimensionless difference $(\Omega_{max} - \Omega_{min})/(k_BT)$ as a function of the shifted dimensionless chemical potential $b \equiv (\mu - \mu_\infty)/(k_BT)$ in liquid argon around an uncharged lyophobic particle at $T = 90$ K, $R_n = 10\sigma$, $\varepsilon_{nf}/\varepsilon_{ff} = 0.2$, $\sigma = 2.53 \cdot 10^{-10}$ m, and $a = 3.58 \cdot 10^{-49}$ J m^3.

Equimolecular radii of stable and unstable concentric nanobubbles were determined[57] symmetrically to Eq. (10) as

$$R_{em}^3 = -\frac{\rho_g}{\rho_l - \rho_g} R_n^3 + \frac{1}{\rho_l - \rho_g} \int_{R_n}^{\infty} dr r^3 \frac{d\rho(r)}{dr}. \qquad (15)$$

These radii increase with an increase in the radius of the lyophobic solid nucleus. Using Eq. (15), the results for the equilibrium density profiles at different chemical potentials of the fluid can be transformed into the dependence of the shifted chemical potential $b_{R_{em}} = (\mu_{R_{em}} - \mu_\infty)/(k_BT)$ per molecule in the concentric vapor shell on radius R_{em} (Fig. 13).[57] It is seen that the curve of the dependence of the chemical potential of molecules in the bubble with the lyophobic nucleus on the bubble radius has a minimum below which the heterogeneous nucleation of bubbles becomes thermodynamically barrierless. The appearance of an electrical charge on the nucleus shifts the chemical potential minimum of the condensate to the lower values and hinders bubble nucleation.

In addition, the dependence of the surface tension γ of a bubble on the radius R_{em} of the equimolecular separating surface and charge of the central lyophobic nucleus at the heterogeneous nucleation of a bubble was studied.[57] A monotonic decrease in

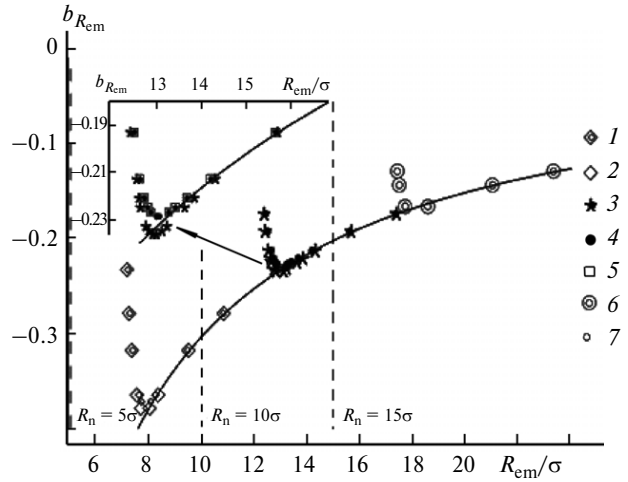

Fig. 13. Shifted dimensionless chemical potential $b_{R_{em}}$ of a molecule of argon vapor in a bubble around the uncharged lyophobic particle *vs* bubble radius calculated at $T = 90$ K and at nucleus radii: $R_n = 5\sigma$ and $\varepsilon_{nf}/\varepsilon_{ff} = 0.2$ (*1*), 0.002 (*2*); $R_n = 10\sigma$ and $\varepsilon_{nf}/\varepsilon_{ff} = 0.2$ (*3*), 0.002 (*4*), 0 (*5*); $R_n = 15\sigma$ and $\varepsilon_{nf}/\varepsilon_{ff} = 0.2$ (*6*), 0.002 (*7*). Solid line shows the behavior of the capillary approximation for the shifted chemical potential at $R_n = 0$. Vertical dashed lines separate the cases with different nucleus radii R_n. Inset: amplified fragment of the plot.

the surface tension for critical bubbles with a decrease in the radius was observed in the range where the results for the profiles of homogeneously and heterogeneously formed bubbles are very close. However, stable bubbles demonstrate the retardation of a decrease in the surface tension and even its increase for the smallest stable bubbles. After removal of the results of the smallest stable bubbles referred to the very thin interlayers, where the solid body—vapor and vapor—liquid interfaces are substantially overlapped, it was shown[57] that the $\gamma(R_{em})$ dependence is described by Eq. (14) with the negative curvature for bubbles $c = -1/R_{em}$. The following Tolman lengths and rigidity constants were obtained at $R_n = 0$ (homogeneous bubble): $\delta_\infty = -0.19\sigma$ and $\varkappa = -1.42\sigma^2$, which is sufficiently close to the values[52] at the same temperature $T = 90$ K and the same thermodynamic parameters for homogeneous argon droplets. The following values were found at $R_n = 10\sigma$, $Z = 0$, and $\varepsilon_{nf}/\varepsilon_{ff} = 0.2$ (heterogeneous bubble): $\delta_\infty = -0.076\sigma$ and $\varkappa = -4.41\sigma^2$; at $R_n = 10\sigma$, $Z = 4$, and $\varepsilon_{nf}/\varepsilon_{ff} = 0.2$ (heterogeneous bubble): $\delta_\infty = -0.076\sigma$ and $\varkappa = -9.53\sigma^2$; and at $R_n = 10\sigma$, $Z = 8$, and $\varepsilon_{nf}/\varepsilon_{ff} = 0.2$ (heterogeneous bubble): $\delta_\infty = -0.076\sigma$ and $\varkappa = -25.2\sigma^2$. It was mentioned[57] that when taking only the points referred to larger bubbles, then the δ_∞ and $\varkappa$ values become closer to those for the homogeneously nucleated bubble. In the general case, it can be expected that the influence of the central electrical field on the surface tension of the vapor bubble is stronger than that in the case of the liquid droplet,[52] since there is no field screening in the bubble. As follows from the presented results,[57] an electrical charge does not affect the Tolman length δ_∞, but the effect of an increase in the electrical charge of the central particle on the effective rigidity constant is already strong. This behavior agrees with the theoretical predictions in the framework of the method of separating Gibbs surfaces.[61]

The influence of the disjoining pressure on the equilibrium form of the free nanobubble or nanobubble fixed on the planar substrate in gas-supersaturated solutions was considered[62] in terms of the film thickness functional method in which the grand thermodynamic potential of a substrate—bubble—liquid system is written as a functional of the profile of the bubble shape for the specified isotherm of disjoining pressure. The discovered[57] radial anisotropy of molecular density in thin equilibrium vapor interlayers regularly arises questions about anisotropy of the pressure tensor in stable heterogeneous bubbles and on the existence of the disjoining pressure in such bubbles. Answers to these questions in terms of the gradient molecular density functional method are given in the works,[58,59] where the profiles of the normal and tangent components of the local pressure tensor were analyzed in argon vapor interlayers near the planar substrate and around the spherical nucleus in stretched liquid argon at several values of chemical potential of argon molecules and parameters determining lyophobicity of the solid body. The calculations showed a significant anisotropy of the normal and tangent components of the pressure tensor near lyophobic solid surfaces. The values of disjoining pressure were calculated with using the mechanical ($\Pi^{(m)}$) and thermodynamical ($\Pi^{(t)}$) definitions, which were written, unlike Eqs (12) and (13), for the spherical interlayer in the form

$$\Pi^{(m)}(R_{em} - R_n) \equiv \left[P_N(r_i) - P_g(\mu)\right]\left(\frac{r_i}{R_n}\right)^2 \qquad (16)$$

and

$$\Pi^{(t)}(h_{em}) = \left(\frac{2\gamma_{em}}{R_{em}} + P_l(\mu) - P_g(\mu)\right)\left(\frac{R_{em}}{R_n}\right)^2. \qquad (17)$$

The mechanically and thermodynamically determined values of disjoining pressure coincide within the limits of inaccuracy, which is mainly determined by using the approximation $\gamma_{em} = \gamma_\infty$ and fixed choice of the point $r_i = R_n + d/2$. The calculation results[59] for the dimensionless mechanically determined pressure $\tilde{\Pi} = \Pi^{(m)}\sigma^3/(k_B T)$ in the planar ($R_n = \infty$) and spherical vapor argon layer around the uncharged spherical lyophobic nucleus at three values of nucleus radius R_n are shown in Fig. 14. A decrease in the disjoining pressure with an increase in the layer thickness (both the planar and spherical cases) indicates the stability of the vapor layers. Interestingly, the smaller the lyophobic particle radius, the higher the disjoining pressure in the spherical bubble on the lyophobic nucleus. Therefore, the disjoining pressure in the planar vapor layer is the lowest among the others. This is contrary to the case of disjoining pressure in liquid films around the lyophilic particle (see Fig. 10). Depending on the degree of lyophobicity, the disjoining pressure isotherms change from nonmonotonic to monotonic functions of the vapor layer thickness.

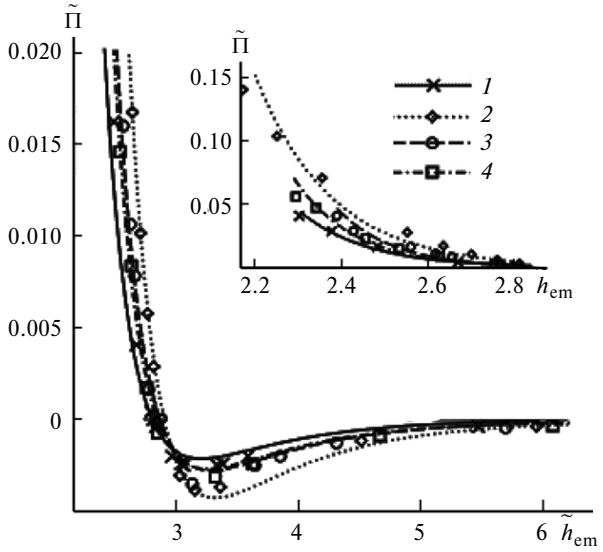

Fig. 14. Dimensionless mechanically determined disjoining pressure $\tilde{\Pi} = \Pi^{(m)}\sigma^3/(k_BT)$ as a function of the dimensionless interlayer thickness $\tilde{h} = (R_{em} - R_n)/\sigma$ in the planar ($R_n = \infty$) (*1*) and spherical vapor layer of argon on the uncharged lyophobic nucleus at three values of the nucleus radius: R_n: 5σ (*2*), 10σ (*3*), and 15σ (*4*). Symbols indicate the calculation results, and curves are analytical approximations. Accepted in calculations: $T = 90$ K, and lyophobicity of the nucleus was specified by the ratio $\varepsilon_{nf}/a = 0.2$, $\sigma = 2.53 \cdot 10^{-10}$ m, and $a = 3.58 \cdot 10^{-49}$ J m^3. Inset: amplified fragment of the plot.

The gradient version of the molecular density functional method inself is a well checked tool for the theoretical study of nonhomogeneous systems with surface layers between solid, liquid, and gas phases.[63,64] The gradient method is also interesting since its results can be extended not only over molecular systems with the central interaction potential but also over systems with polar molecules and noncentral interactions. However, a number of principal questions still remains in terms of the gradient method concerned with its application for very thin vapor interlayers. These questions are associated with boundary conditions imposed on the density profile near the solid surface,[41,65–68] with inaccuracy of the gradient method depending on the interlayer thickness, and the role of the explicit representation for the intermolecular chemical potential. Some answers to these questions were obtained[60] in the study of extremes of the grand thermodynamic potential of a solid lyophobic nucleus—vapor interlayer—stretched liquid system using the elastic band method[69–73] and integral nonlocal density functional method.[34,35] As applied to the nucleation problem, elastic band pushing is the method of investigation of the relief of the grand thermodynamic potential as a functional in the space of density profiles *via* the optimization of chains of the states of the system, which are characterized by the values of the grand thermodynamic potential accepted in them on going from the initial metastable phase state to the final state with the new phase particle.[72,73] The initial states of the system and corresponding initial values of the grand thermodynamic potential at each number *i* are specified by its starting density profile. In this approach, the solution of the corresponding Euler equation for the functional of the grand thermodynamic potential is not required and, correspondingly, it is not necessary to impose boundary conditions on the density profiles on the nucleus surface. As a result, this method makes it possible to find the path of the minimal difference in the grand thermodynamic potential that "is passed" by the system on going from the initial unstable state to the final stable state. Reaching of such a path according to the calculations[60] is shown in Fig. 15.

Here the grand thermodynamic potential Ω of a lyophobic nucleus—vapor interlayer—stretched liquid system is specified by Eqs (6)—(9), and the calculations were performed for argon and paraffin

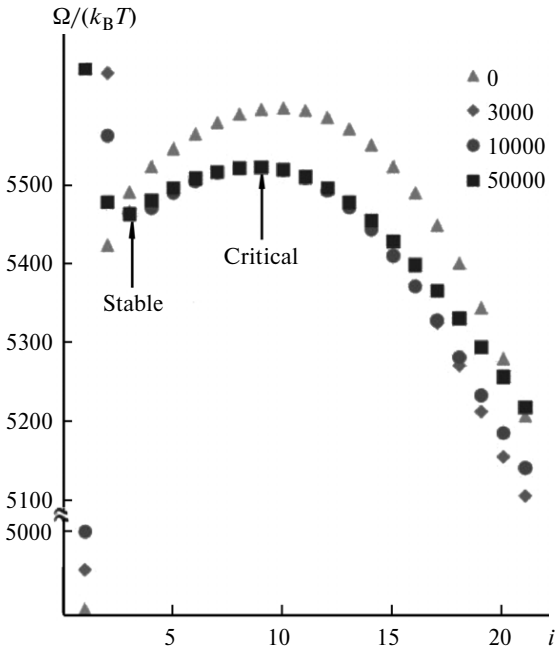

Fig. 15. Initial, two intermediate (3000 and 10 000 steps), and final (50 000 steps, minimal grand potential difference path) chains of the states for the bubble around the lyophobic particle ($N = 21$ is the number of states in the chain, $T = 90$ K, $R_n = 10\sigma$, $\varepsilon_{nf} = 0.01a/\sigma^3$, $\rho_n = 1.07 \cdot 10^{27}$ m^{-3}, $(\mu - \mu_\infty)/(k_BT) = -0.193$, $\sigma = 2.53 \cdot 10^{-10}$ m, and $a = 3.58 \cdot 10^{-49}$ J m^3).

nucleus. As can be seen from Fig. 15, the optimum curve $\Omega(i)$ has local minimum and maximum corresponding to the minimum and maximum of functional Ω. Thus, a stable vapor bubble around a lyophobic particle also exists in the elastic strip model. The agreement of the equilibrium density profiles corresponding to the extremes on the optimum curve $\Omega(i)$ and solutions in the gradient density functional method is very good, and the difference in the Ω values obtained by both methods at the minimum and saddle point does not exceed 0.001. Although the boundary conditions in the elastic band method are not specified, but the density profiles obtained in terms of this method, as a result, satisfy the boundary conditions $\rho(R_n + d/2) = 0$ and $\rho(r)|_{r\to\infty} = \rho_l$.

A more general problem about finding equilibrium profiles of bubbles on solid particles of arbitrary lyophobicity was considered[74] in the framework of the elastic strip method. In this study, no minimum in the form of a bubble was observed on the obtained optimum curve $\Omega(i)$. However, it should be mentioned that the nonlocal integral density functional method was used in that work in combination with taking into account correlations of solid spheres. To check whether the presence of the minimum is an artifact of the gradient method of the molecular density functional method, the density profiles were found[60] for the free concentric bubble around the lyophobic particle using the nonlocal integral method. The distinction of the integral density functional method is that, in the random phase approximation, the grand thermodynamic potential Ω for the particle—shell—liquid system can be presented as follows:

$$\Omega = \int d\vec{r}\left[f_{hs}(\rho) - \mu\rho + \rho w_{nf}(r)\right] + \\ + \frac{1}{2}\int d\vec{r}\int d\vec{r}\, w(|\vec{r} - \vec{r}\,'|)\rho(\vec{r})\rho(\vec{r}\,'). \qquad (18)$$

In the calculations in Ref. 60, neglecting the correlations of solid spheres, which should not be substantial for the formation of bubbles on lyophobic particles, the free energy density of solid spheres $f_{hs}(\rho)$ and potential $w_{nf}(r)$ of interaction of the nucleus with the fluid molecule were taken the same as those in Eqs (8) and (9). The central attraction potential between fluid molecules $w(|\vec{r} - \vec{r}\,'|)$ was taken in the form of the Yukawa potential $w_Y(r) = -\frac{ad^2}{2\pi}\frac{e^{-dr}}{r}$, where d is the diameter of the molecule, and a is the attraction parameter of fluid molecules in the mean-field approximation (the same as that in Eq. (6)) and as the Lennard-Jones potential in the Weeks—Chandler—Andersen form[34,35]:

$$w_{LJ}(r) = \begin{cases} -\varepsilon_{ff}, & r < 2^{1/6}\sigma_{LJ} \\ 4\varepsilon_{ff}\left[\left(\frac{\sigma_{LJ}}{r}\right)^{12} - \left(\frac{\sigma_{LJ}}{r}\right)^{6}\right], & r > 2^{1/6}\sigma_{LJ}, \end{cases} \qquad (19)$$

where ε and σ_{LJ} are the parameters of the Lennard-Jones potential ($\sigma_{LJ} \neq \sigma$). Parameters a and C in Eq. (6) are related *via* the second and fourth integral moments of the long-range central potential, respectively.[60,76] If taking $\varepsilon_{ff} \cong 0.630a/d^3$ and $\sigma_{LJ} \cong 0.5856d$, then both intermolecular potentials give the same contributions to the grand thermodynamic potential Ω in the gradient density functional method.

A comparison of the density profiles of the vapor interlayer and bulk liquid obtained by the solution[60] of the variation problem $\delta\Omega[\rho(\vec{r})]/\delta\rho(\vec{r}) = 0$ with functionals (6) and (18) is shown in Fig. 16. It is seen that the stable vapor interlayers corresponding to the minimum of the grand thermodynamic potential of the system exist in terms of the integral method for both models of intermolecular potential. The gradient method increases the bubble radius and makes its density profile flatter. The profiles of critical vapor interlayers do not virtually differ from the profiles of homogeneous bubbles. The profiles of the stable vapor interlayers do not reach zero at $r = R_p + d/2$

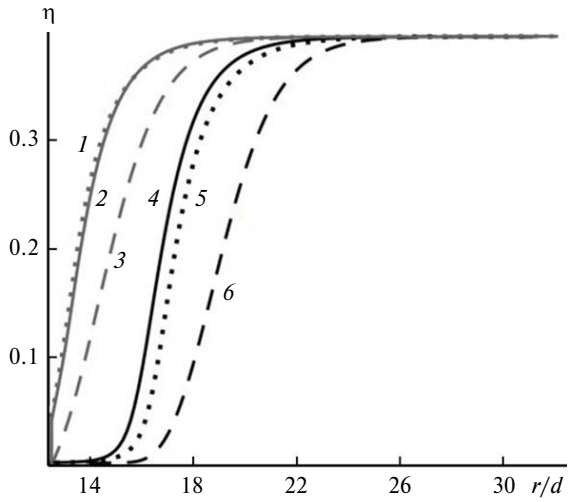

Fig. 16. Density profiles of stable (curves *1*—*3*) and critical (curves *4*—*6*) vapor interlayers for fluids with the Yukawa potential (*1*, *5*), with the Lennard-Jones potential (*2*, *4*), and in comparison with the profiles for the gradient method (*3*, *6*). Accepted in calculations: $T = 90$ K, $R_p = 10d$, $\varepsilon_{nf} = 0.01a/\sigma^3$, $\rho_n = 1.07 \cdot 10^{27}$ m^{-3}, $(\mu - \mu_\infty)/(k_B T) = -0.275$, and $a = 3.58 \cdot 10^{-49}$ J m^3.

as it takes place for the gradient method. This distinction was observed previously[41] for the fluid near the planar wall possessing only an infinitely high repulsion potential.

When describing nanodroplets or nanobubbles in the framework of the molecular density functional method and taking into account the repulsion of molecules, the local density of the free energy for the equilibrium system of solid spheres should be specified with high accuracy as a function of the local density of the number of particles. The questions arise how strong is the difference between the molecular density profiles in radially nonuniform spherical small droplets and bubbles and what is the dependence of the surface tension of droplets and bubbles on their size when different equations of state are used for the description of local contributions of solid spheres to the grand thermodynamic potential of the molecular fluid? The molecular density profiles in radially nonuniform spherical small droplets and bubbles obtained in terms of the molecular density functional method for several high-accuracy models of the free energy density of solid spheres has recently been compared[76] for argon. The models following from the Carnahan—Starling equation of state,[44] truncated 6th-order Rusanov′s equation,[77] and virial expansion with eighteen coefficients[78] were considered. It was shown that the choice of the equation of state affected the values characterizing the two-phase equilibrium, for example, the value of chemical potential or surface tension for the planar interface between the phases and can shift the size of the droplet or bubble.

Conclusion

The present review considers the results of the theoretical study of the thermodynamic and structural characteristics of free droplets and bubbles around solid nanoparticles obtained in terms of both the phenomenological thermodynamic approach and different versions of the molecular density functional method. It is shown that, for condensation in undersaturated or supersaturated vapor, the well wettable solid spherical nanoparticle plays the role of a condensation nucleus on which a thermodynamically stable droplet consisted of a thin liquid film around the nucleus can be formed due to the disjoining pressure in the liquid film. The presence of an electrical charge on the condensation nucleus enhances its nucleation activity, decreases the chemical potential of molecules in the droplet, and increases the liquid film thickness of the stable droplet. The phenomenological theory[1—3,6—11] and results obtained by the molecular density functional method[42,43,46,47] are well consistent for stable droplets with uncharged and uniformly charged condensation nucleus. It is shown that the classical theory of nucleation on charged nuclei based on J. J. Thomson equation[12] is inappropriate in the case of strong wetting of the nucleus. In the case of bubbles, the calculations in terms of the density functional method confirm the role of strongly lyophobic particles as nuclei for stable bubbles in the stretched liquid.[57,60] The thermodynamic and mechanical determinations of the disjoining pressure in stable thin interlayers nearly coincide for the calculations from the density profiles and normal component of the pressure tensor. The disjoining pressures in stable spherical liquid droplets increase[47] with an increase in the nucleus size, whereas in vapor films they decrease.[58,59] It is shown[60] that the stable equilibrium density profiles found in terms of the gradient method of molecular density functional in concentric vapor shells around non-wettable nanoparticles in the liquid phase also exist in terms of the integral density functional method and elastic band method. A specific choice of various equations of state for a system of solid spheres to determine the explicit form of the grand thermodynamic potential in the molecular density functional method affects[76] the values characterizing the two-phase equilibrium but only slightly affects the calculated density profiles and coefficients of the dependence of the surface tension of stable droplets or bubbles on the curvature of their surface.

A promising trend for further studies of stable nanodroplets and nanobubbles is the transition from diverse versions of the molecular density method to problems with sessile droplets and bubbles in which the density profiles stop to be spherically symmetric.[74] Solid particles that can possess an arbitrary wettability is of interest in this respect.

The study was financially supported by the Russian Science Foundation (Project No. 22-13-00151, https://rscf.ru/project/22-13-00151/).

No human or animal subjects were used in this research.

The authors declare no competing interests.

References

1. A. I. Rusanov, F. M. Kuni, *Dokl. Akad. Nauk SSSR* [*Proc. Acad. Sci. USSR*], 1991, **318**, 1410 (in Russian).
2. A. I. Rusanov, F. M. Kuni, *Colloids Surf.*, 1991, **61**, 349; DOI:10.1016/0166-6622(91)80320-N.
3. A. I. Rusanov, *Russ. J. Gen. Chem.*, 2022, **92**, 539; DOI: 10.1134/S1070363222040016.
4. B. V. Derjaguin, N. V. Churaev, V. M. Muller, *Surface Forces*, Consultants Bureau, New York, 1987.
5. A. I. Rusanov, F. M. Kuni, A. K. Shchekin, *Colloid J.* (*Engl. Transl.*), 1994, **56**, 172.
6. F. M. Kuni, A. K. Shchekin, A. I. Rusanov, B. Widom, *Adv. Colloid Interface Sci.*, 1996, **65**, 71; DOI: 10.1016/0001-8686(96)00290-4.
7. F. M. Kuni, A. K. Shchekin, A. P. Grinin, *Phys.-Usp.*, 2001, **44**, 331; DOI: 10.1070/PU2001v044n04ABEH000783.
8. A. K. Shchekin, D. V. Tatyanenko, F. M. Kuni, in *Nucleation Theory and Applications*, Eds J. W. P. Schmelzer, G. Röpke, V. B. Priezzhev, JINR, Dubna, 1999, p. 320.
9. D. V. Tatyanenko, A. K. Shchekin, F. M. Kuni, *Colloid J.* (*Engl. Transl.*), 2000, **62**, 479.
10. J. Mitrovic, *Chem. Eng. Sci.*, 2006, **61**, 5925; DOI: 10.1016/j.ces.2006.05.013.
11. A. K. Shchekin, T. S. Podguzova, *Atmos. Res.*, 2011, **101**, 493; DOI: 10.1016/j.atmosres.2010.10.006.
12. J. J. Thomson, G. P. Thomson, *Conduction of Electricity Through Gases*, Cambridge University Press, London, 1928.
13. V. B. Warshavsky, T. S. Podguzova, D. V. Tatyanenko, A. K. Shchekin, *J. Chem. Phys.*, 2013, **138**, 194708; DOI: 10.1063/1.4804655.
14. V. B. Warshavsky, T. S. Podguzova, D. V. Tatyanenko, A. K.Shchekin, *Colloid J.* (*Engl. Transl.*), 2013, **75**, 504; DOI: 10.1134/S1061933X13050153.
15. A. I. Rusanov, A. K. Shchekin, *Colloid J.* (*Engl. Transl.*), 2005, **67**, 205; DOI: 10.1007/s10595-005-0082-8.
16. A. I. Rusanov, A. K. Shchekin, *Mol. Phys.*, 2005, **103**, 2911; DOI: 10.1080/00268970500151510.
17. A. V. Nguyen, H. J. Schulze, *Colloidal Science of Flotation*, Marcel Dekker Inc., New York, 2004.
18. I. Mackay, A. R. Videla, P. R. Brito-Parada, *J. Clean. Prod.*, 2020, **242**, 118436; DOI: 10.1016/j.jclepro.2019.118436.
19. C. Li, H. Zhang, *Powder Technol.*, 2022, **395**, 618; DOI: 10.1016/j.powtec.2021.10.004.
20. A. I. Rusanov, *Russ. Chem. Rev.*, 1964, **33**, 385.
21. A. J. M. Yang, *J. Chem. Phys.*, 1985, **82**, 2082; DOI: 10.1063/1.448344.
22. H. Ulbricht, J. Schmelzer, R. Mahnke, F. Schweitzer, *Thermodynamics of Finite Systems and the Kinetics of First-Order Phase Transitions*, Teubner, Leipzig, 1988.
23. J. Schmelzer, *Z. Phys. Chemie*, 1988, **269**, 633; DOI: 10.1515/zpch-1988-26968.
24. A. V. Neimark, A. Vishnyakov, *J. Chem. Phys.*, 2005, **122**, 05470; DOI: 10.1063/1.1829040.
25. L. G. MacDowell, V. K. Shen, J. R. Errington, *J. Chem. Phys.*, 2006, **125**, 034705; DOI: 10.1063/1.2218845.
26. Ø. Wilhelmsen, D. Reguera, *J. Chem. Phys.*, 2015, **142**, 064703; DOI: 10.1063/1.4907367.
27. T. Philippe, *Phys. Rev. E*, 2017, **96**, 032802; DOI: 10.1103/PhysRevE.96.032802.
28. A. K. Shchekin, K. Koga, N. A. Volkov, *J. Chem. Phys.*, 2019, **151**, 244903; DOI: 10.1063/1.5129160.
29. J. H. Weijs, D. Lohse, *Phys. Rev. Lett.*, 2013, **110**, 054501; DOI: 10.1103/PhysRevLett.110.054501.
30. Y. W. Liu, X. H. Zhang, *J. Chem. Phys.*, 2013, **138**, 014706; DOI: 10.1063/1.4773249.
31. D. Lohse, X. H. Zhang, *Phys. Rev. E*, 2015, **91**, 031003; DOI: 10.1103/PhysRevE.91.031003.
32. M. Alheshibri, J. Qian, M. Jehannin, V. S. J. Craig, *Langmuir*, 2016, **32**, 11086; DOI: 10.1021/acs.langmuir.6b02489.
33. P. Attard, *Langmuir*, 2016, **32**, 11138; DOI: 10.1021/acs.langmuir.6b01563.
34. R. Evans, in *Fundamentals of Inhomogeneous Fluids*, Marcel Dekker, New York, 1992, Ch. 3, p. 85.
35. J. F. Lutsko, *Adv. Chem. Phys.*, 2010, **144**, 1; DOI: 10.1021/acs.langmuir.6b01563.
36. V. Talanquer, D. W. Oxtoby, *J. Chem. Phys.*, 1996, **104**, 1483; DOI: 10.1063/1.470914.
37. T. V. Bykov, X. C. Zeng, *J. Chem. Phys.*, 2002, **117**, 1851; DOI: 10.1063/1.1485733.
38. I. Napari, A. Laaksonen, *J. Chem. Phys.*, 2003, **119**, 10363; DOI: 10.1063/1.1619949.
39. H. Kitamura, A. Onuki, *J. Chem. Phys.*, 2005, **123**, 124513; DOI: 10.1063/1.2039078.
40. T. V. Bykov, X. C. Zeng, *J. Chem. Phys.*, 2006, **125**, 144515; DOI: 10.1063/1.2357937.
41. E. M. Blokhuis, J. Kuipers, *J. Chem. Phys.*, 2007, **126**, 054702; DOI: 10.1063/1.2434161.
42. A. K. Shchekin, T. S. Lebedeva, D. V. Tatyanenko, *Fluid Phase Equilib.*, 2016, **424**, 162; DOI: 10.1016/j.fluid.2016.02.025.
43. A. K. Shchekin, T. S. Lebedeva, D. V. Tatyanenko, *Colloid J.* (*Engl. Transl.*), 2016, **78**, 553; DOI: 10.1134/S1061933X16040165.
44. N. F. Carnahan, K. E. Starling, *J. Chem. Phys.*, 1969, **51**, 635; DOI: 10.1063/1.1672048.
45. V. V. Zubkov, I. V. Grinev, V. M. Samsonov, *Nanosistemy: fizika, khimiya, matematika* [*Nanosystems: Physics*, *Chemistry, Mathematics*], 2012, **3**, No. 3, 52 (in Russian).
46. A. K. Shchekin, T. S. Lebedeva, *J. Chem. Phys.*, 2017, **146**, 094702; DOI: 10.1063/1.4977518.
47. A. K. Shchekin, T. S. Lebedeva, D. Suh, *Colloids Surf. A*, 2019, **574**, 78; DOI: 10.1016/j.colsurfa.2019.04.071.

48. A. K. Shchekin, I. V. Shabaev, A. I. Rusanov, *J. Chem. Phys.*, 2008, **129**, 214111; DOI: 10.1063/1.3021078.
49. A. K. Shchekin, I. V. Shabaev, O. Hellmuth, *J. Chem. Phys.*, 2013, **138**, 054704; DOI: 10.1063/1.4789309.
50. O. Hellmuth, A. K. Shchekin, *Atmos. Chem. Phys.*, 2015, **15**, 3851; DOI: 10.5194/acp-15-3851-2015.
51. A. K. Shchekin, A. I. Rusanov, *J. Chem. Phys.*, 2008, **129**, 154116; DOI: 10.1063/1.2996590.
52. T. S. Lebedeva, D. Suh, A. K. Shchekin, *Mech. Solids*, 2020, **55**, 55; DOI: 10.3103/S0025654420010161.
53. V. G. Baidakov, G. Sh. Boltachev, *Phys. Rev. E*, 1999, **59**, 469; DOI: 10.1103/PhysRevE.59.469.
54. T. V. Bykov, A. K. Shchekin, *Inorg. Mater.*, 1999, **35**, 641.
55. E. M. Blokhuis, A. E. van Giessen, *J. Phys.: Condens. Matter*, 2013, **25**, 225003; DOI: 10.1088/0953-8984/25/22/225003.
56. Ø. Wilhelmsen, D. Bedeaux, D. Reguera, *J. Chem. Phys.*, 2015, **142**, 064706; DOI: 10.1063/1.4907588.
57. A. K. Shchekin, L. A. Gosteva, T. S. Lebedeva, *Physica A*, 2020, **560**, 125105; DOI: 10.1016/j.physa.2020.125105.
58. A. K. Shchekin, L. A. Gosteva, T. S. Lebedeva, D. V. Tatyanenko, *Colloid J.* (*Engl. Transl.*), 2021, **83**, 263; DOI: 10.1134/S1061933X21010129.
59. A. Shchekin, L. Gosteva, D. Tatyanenko, *Colloids Surf. A*, 2021, **615**, 126277; DOI: 10.1016/j.colsurfa.2021.126277.
60. L. A. Gosteva, A. K. Shchekin, *Colloid J.* (*Engl. Transl.*), 2021, **83**, 558; DOI: 10.1134/S1061933X21050045.
61. F. M. Kuni, A. K. Shchekin, A. I. Rusanov, *Colloid J. USSR*, 1983, **45**, 598.
62. V. B. Svetovoy, I. Dević, J. H. Snoeijer, D. Lohse, *Langmuir*, 2016, **32**, 11188; DOI: 10.1021/acs.langmuir.6b01812.
63. J. F. Lutsko, *J. Chem. Phys.*, 2011, **134**, 164501; DOI: 10.1063/1.3582901.
64. V. G. Baidakov, *J. Chem. Phys.*, 2016, **144**, 074502; DOI: 10.1063/1.4941689.
65. H. Nakanishi, M. E. Fisher, *Phys. Rev. Lett.*, 1982, **49**, 1565; DOI: 10.1103/PhysRevLett.49.1565.
66. J. O. Indekeu, K. Ragil, D. Bonn, D. Broseta, J. Meunier, *J. Stat. Phys.*, 1999, **95**, 1009; DOI: 10.1023/A:1004558618646.
67. K. Padilla, V. Talanquer, *J. Chem. Phys.*, 2001, **114**, 1319; DOI: 10.1063/1.1332995.
68. L. M. Pismen, Y. Pomeau, *Phys. Rev. E*, 2000, **62**, 2480; DOI: 10.1103/PhysRevE.62.2480.
69. G. Henkelman, B. P. Uberuaga, H. Jonsson, *J. Chem. Phys.*, 2000, **113**, 9901; DOI: 10.1063/1.1329672.
70. G. Henkelman, H. Jonsson, *J. Chem. Phys.*, 2000, **113**, 9978; DOI: 10.1063/1.1323224.
71. E. Bitzek, P. Koskinen, F. Gähler, M. Moseler, P. Gumbsch, *Phys. Rev. Lett.*, 2006, **97**, 170201; DOI: 10.1103/PhysRevLett.97.170201.
72. D. Sheppard, R. Terrell, G. Henkelman, *J. Chem. Phys.*, 2008, **128**, 134106; DOI: 10.1063/1.2841941.
73. J. F. Lutsko, *J. Chem. Phys.*, 2008, **129**, 244501; DOI: 10.1063/1.3043570.
74. D. Huang, X. Quan, P. Cheng, *Int. Commun. Heat Mass Transfer*, 2018, **93**, 66; DOI: 10.1016/j.icheatmasstransfer.2018.03.005.
75. B. Q. Lu, R. Evans, M. M. Telo da Gama, *Mol. Phys.*, 1985, **55**, 1319; DOI: 10.1080/00268978500102041.
76. A. K. Shchekin, D. V. Tatyanenko, L. A. Gosteva, K. D. Apitsin, *Russ. J. Gen. Chem.*, 2022, **92**, 629; DOI: 10.1134/S1070363222040041.
77. A. I. Rusanov, *Russ. Chem. Rev.*, 2005, **74**, 126; DOI: 10.1070/RC2005v074n02ABEH000970.
78. J. Hu, Y.-X. Yu, *Phys. Chem. Chem. Phys.*, 2009, **11**, 9382; DOI: 10.1039/b911901a.

Received May 22, 2022;
in revised form June 30, 2022;
accepted July 7, 2022